PHYSICAL REVIEW B **95**, 201113(R) (2017)

Observation of bound and antibound states of two excitons in GaAs single quantum well by two-dimensional coherent spectroscopy

Y. Ogawa*

Department of Physics, Joetsu University of Education, Yamayashiki-machi 1, Joetsu-shi, Niigata 943-8512, Japan

(Received 17 November 2016; revised manuscript received 3 May 2017; published 23 May 2017)

We study the bound and antibound states of two excitons in a GaAs single quantum well by two-dimensional coherent spectroscopy. We also propose a method to directly observe the amplitude and phase (real and imaginary parts) of optical fields by using a heterodyne interference technique and through synchronized detection of the interference signals. In this scheme, the mechanical fluctuation of an unstabilized interferometer does not affect the measurement. In addition, the amplitude and phase of the optical fields, resulting from the coherent interactions between light and matter, are directly obtained by comparing a reference heterodyne beating signal by using a two-phase lock-in amplifier. By using this method, the bound and antibound states of two excitons are observed. It is expected that the excitons are localized to the quantum islands and the lateral confinement induces the large repulsive energy between the two excitons.

DOI: 10.1103/PhysRevB.95.201113

Two-dimensional coherent spectroscopy (2DCS) is a powerful tool for investigating the many-body interactions of atoms, molecules, and condensed matter [1,2]. For example, the coherent coupling of molecular vibrations and the coherent interaction between the photoexcited carriers show a complex time evolution. 2DCS is capable of revealing the interactions as individual peaks in a 2D map. In contrast, conventional one-dimensional (1D) spectroscopy cannot separate each interaction.

We focus on the many-body interactions among excitons in semiconductors, especially the bound and antibound states of two excitons, in this Rapid Communication. The bound and antibound two-exciton states are composed of opposite-spin and same-spin excitons, respectively, and the interactions between excitons and multiexcitons contribute to the dephasing process in semiconductors [3,4]. It is, however, difficult to observe the antibound states due to the small repulsive energy. It is expected that the multiexciton states are investigated in detail by using the 2DCS because of the ability to separate the interactions as individual peaks.

In 2DCS, coherently controlled pulse sequences excite a sample, and a four-wave mixing (FWM) signal is generated because of the nonlinear interactions in the sample. The FWM signal is generated along the direction of $-\boldsymbol{k}_1+\boldsymbol{k}_2+\boldsymbol{k}_3$, where $\boldsymbol{k}_1$, $\boldsymbol{k}_2$, and $\boldsymbol{k}_3$ are the wave vectors of the first, second, and third excitation pulses, respectively. The signal field, that is, the third-order coherent field, is diffracted by spatial second-order population grating with a wave vector of $\boldsymbol{k}_2-\boldsymbol{k}_1$. Therefore, the excitation process of $\boldsymbol{k}_1$ and $\boldsymbol{k}_2$ pulses corresponds to the absorption process that depends on the delay and the relative phase between the two pulses: The generation of the diffracted signal is understood as the emission process from the excited states. The amplitude and phase of the FWM signal are measured by interfering with a reference pulse. 2D spectra are then obtained by taking a numerical Fourier transform of the complex FWM signal in the time domains of both the absorption and emission processes. Therefore, 2DCS reveals the correlation between the two processes.

However, 2DCS faces certain complications. First, the pulse sequences must be generated through subwavelength phase stabilization. One method involves pulse shaping by using spatial light modulators and phase masks [5–7]. As the pulse delays are shorter than the coherence times of the semiconductor nanomaterials [8,9], it is difficult to apply 2DCS to semiconductor physics. In the second method, the pulses are generated using an interferometer, through which a continuous wave laser is passed to actively stabilize it [10–12]. However, the experimental setup is complicated and large scale compared to the pulse shaping experiment.

The second difficulty arises in obtaining the amplitude and phase of the signal field. In a well-known method, the interference patterns in a frequency domain between the signal and reference optical fields are measured using a spectrometer [11]. Complicated calculations are then necessary to obtain the amplitude and phase. These methods are an indirect measurement in the sense that calculations are necessary to reconstruct the amplitude and phase.

Furthermore, performing 2DCS of single nano-objects is difficult because they are smaller than the resonant wavelength. It is impossible to determine the signal field of single nano-objects by using the signal wave vector of the FWM, such as $-\boldsymbol{k}_1+\boldsymbol{k}_2+\boldsymbol{k}_3$.

In this Rapid Communication, a method is proposed to avoid the aforementioned difficulties in 2DCS. Each excitation pulse is frequency shifted by acousto-optic modulators (AOMs). The heterodyne interference signals between the signal and reference fields are analyzed by comparing the reference heterodyne beating signal generated by the excitation pulses. In this method, the amplitude and phase of the signal field are directly obtained using a standard lock-in detection technique when the reference heterodyne beating signal is used to synthesize the reference frequencies for a lock-in amplifier (LIA). This setup removes the influence of the mechanical fluctuations of the interferometer without active stabilization. In addition, there is an extensibility for nano-objects because of the coaxial geometry. Similar methods of 2DCS are reported by detecting the photoluminescence [13,14] and photocurrents [15,16] as signals, in which the excitation pulses are modulated by AOMs and the fourth-order populations are detected by

*ogawa@juen.ac.jp

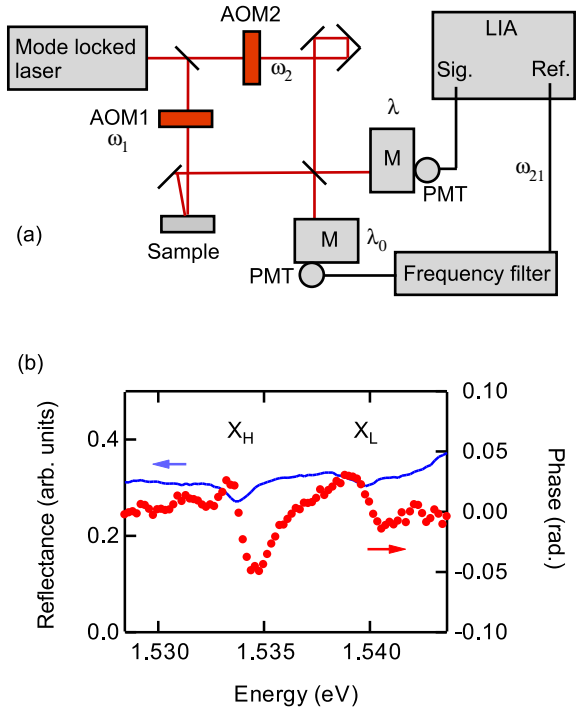

FIG. 1. (a) Experimental setup to obtain the amplitude and phase of the reflected light field of a sample. LIA: lock-in amplifier; AOM: acousto-optic modulator; M: monochromator; PMT: photomultiplier. AOM shifts the frequency of the laser pulses by ω_1 and ω_2, respectively. $\omega_{21} = \omega_2 - \omega_1$ is the beat frequency of the heterodyne interference. (b) Reflectance and phase of a GaAs SQW with a well thickness of 15 nm at 4 K. X_H and X_L indicate heavy- and light-hole excitons, respectively.

LIAs. It can be said that our approach is an evolution of the previous reports. By using this method, we observe the bound and antibound states of two excitons in a GaAs single quantum well (SQW). We discuss the origin of the large repulsive energy of the antibound states.

First, the method to obtain the amplitude and phase of optical fields by using unstabilized interferometers is presented. A mode-locked Ti:sapphire laser that delivers a train of pulses is used. The pulse width and repetition rate are 100 fs and 76 MHz, respectively. The frequency domain comprises a frequency comb of 76 MHz. The train of pulses are separated into first and second pulses by using a Mach-Zehnder interferometer, as shown in Fig. 1(a). Each arm of the interferometer contains an acousto-optic modulator (AOM) that shifts the frequency of the first and second pulses, for example, by $\omega_1 = 40.000$ MHz and $\omega_2 = 40.006$ MHz, respectively. Further, the first diffracted light of the AOMs is used. The first and second light fields are described as

$$\tilde{E}_1(\omega) = \tilde{r}(\omega)E_1(\omega)\exp[i(\omega+\omega_1)t + i\phi_1(\omega) + 2\pi i l_1/\lambda],$$
$$\tilde{E}_2(\omega) = E_2(\omega)\exp[i(\omega+\omega_2)t + i\phi_2(\omega) + 2\pi i l_2/\lambda], \quad (1)$$

where ω and λ are the angular frequency and wavelength of one comb line of the laser pulse, respectively. E_1 (E_2), ϕ_1 (ϕ_2), and l_1 (l_2) are respectively the amplitude, phase, and optical length of each arm of the interferometer. Further, $\tilde{r}(\omega) = r(\omega)\exp[i\phi_r(\omega)]$ is the complex reflectance of the sample. Note that l_1 and l_2 contain the information of the delay between the two pulses.

Two photomultiplier tubes (PMTs) are used to detect the interference signal after each monochromator. The signal is described as follows,

$$\begin{aligned} I(\omega) &= |\tilde{E}_1(\omega) + \tilde{E}_2(\omega)|^2 \\ &= r^2(\omega)E_1^2(\omega) + E_2^2(\omega) + 2r(\omega)E_1(\omega)E_2(\omega) \\ &\quad \times \cos[\omega_{21}t - \phi_r(\omega) + \phi_{21}(\omega) + 2\pi l_{21}/\lambda], \end{aligned} \quad (2)$$

where $\omega_{21} = \omega_2 - \omega_1 = 6$ kHz, $\phi_{21}(\omega) = \phi_2(\omega) - \phi_1(\omega)$, and $l_{21} = l_2 - l_1$. The phase of the heterodyne beating signal contains the phase of the optical field. The phase noise $2\pi\delta l_{21}/\lambda$ is induced by δl_{21}, which is the mechanical fluctuation of the interferometer. In general, stabilization of the interferometer is necessary to measure the phase of the optical fields.

The wavelength (angular frequency) of the reference monochromator is fixed at λ_0 (ω_0), and the signal through a frequency filter, oscillating with a frequency of ω_{21}, is used as the reference of an LIA. The reference is written as $I_{\rm ref} = \cos[\omega_{21}t - \phi_r(\omega_0) + \phi_{21}(\omega_0) + 2\pi l_{21}/\lambda_0]$. The LIA measures the amplitude and relative phase of the signal synchronized with the reference. Therefore, the amplitude $A(\omega)$ and phase $\Phi(\omega)$ of the LIA are written as

$$A(\omega) \propto r(\omega)E_1(\omega)E_2(\omega), \quad (3)$$

$$\begin{aligned} \Phi(\omega) &= -\Delta\phi_r(\omega) + \Delta\phi_{21}(\omega) - 2\pi l_{21}\Delta\lambda/\lambda\lambda_0 \\ &\sim -\Delta\phi_r(\omega) + \Delta\phi_{21}(\omega) \end{aligned} \quad (4)$$

where $\Delta\phi_r(\omega) = \phi_r(\omega) - \phi_r(\omega_0)$, $\Delta\phi_{21}(\omega) = \phi_{21}(\omega) - \phi_{21}(\omega_0)$, and $\Delta\lambda = \lambda - \lambda_0$. The delay is set at $l_{21} = 0$. The phase noise $2\pi\delta l_{21}/\lambda$ is suppressed by using the factor of $\Delta\lambda/\lambda_0$, which is less than 10^{-2} in the experimental condition. By comparing to the amplitude $A_0(\omega) \propto E_1(\omega)E_2(\omega)$ and phase $\Phi_0(\omega) = \Delta\phi_{21}(\omega)$ of a mirror, the amplitude reflectance $r(\omega)$ and relative phase $\Delta\phi_r(\omega)$ of the sample are obtained.

Figure 1(b) shows the reflectance and phase spectra of a GaAs SQW at 4 K. The references $A_0(\omega)$ and $\Phi_0(\omega)$ are obtained using a Cr-coated mirror in which the reflectance and phase are constant. There are two dips in the reflectance in the energy of the heavy-hole (X_H) and light-hole (X_L) excitons. In addition, the phase is modulated by 0.050 rad (2.9°) at the energy of X_H. As the reflected light of the sample mainly comes from the GaAs substrate with no structure in this region, the phase change of the reflection of the SQW is small compared to that of the transmission of thin films and the reflection of bulks [17,18]. The phase error was less than 0.01 rad (0.57°). The estimated error is the result of the fluctuation of the excitation laser, mechanical fluctuation of the interferometer, and electrical noise of the detectors.

Next, I describe the method to obtain the nonlinear signal in the 2DCS. Figure 2(a) indicates the experimental setup [19]. Light-matter interactions in condensed matter cause some nonlinear processes. For example, the FWM signal is written as

$$\tilde{E}^{(3)}_{\rm sig}(\omega) = \tilde{\chi}^{(3)}(\omega)\tilde{E}_1^*(\omega)\tilde{E}_2(\omega)\tilde{E}_3(\omega), \quad (5)$$

where $\tilde{\chi}^{(3)}(\omega) = \chi^{(3)}(\omega)\exp[i\phi^{(3)}(\omega)]$ is the third-order nonlinear susceptibility. Although it is not explicitly indicated,

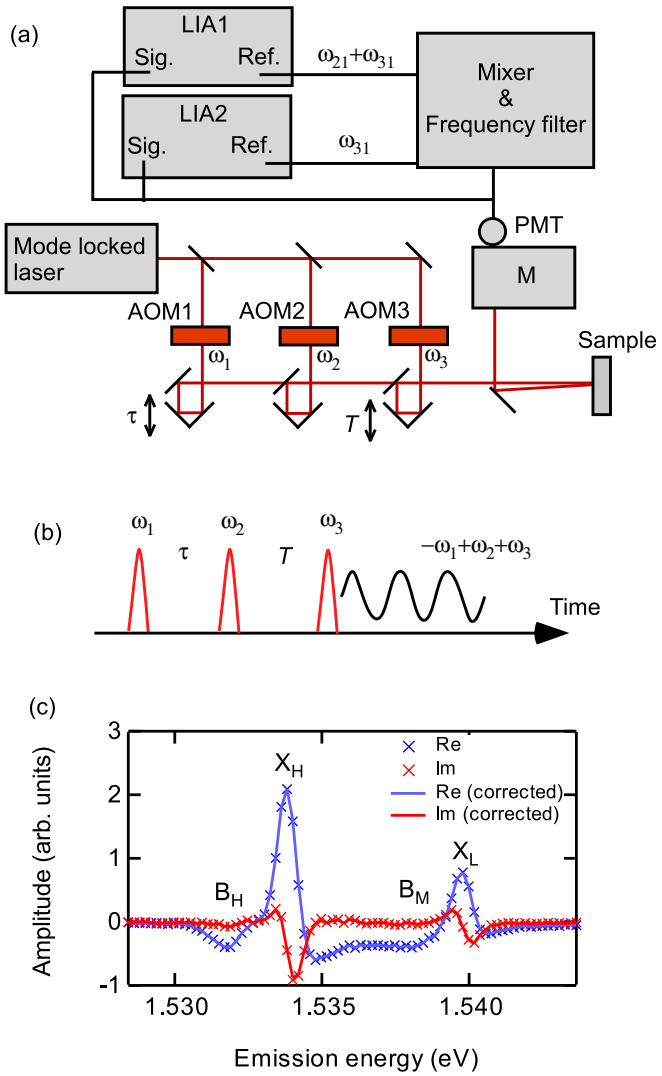

FIG. 2. (a) Experimental setup for 2DFT spectroscopy. LIA: lock-in amplifier; AOM: acousto-optic modulator; M: monochromator; PMT: photomultiplier. AOM shifts the frequency of the laser pulses by ω_1, ω_2, and ω_3. $\omega_{21} = \omega_2 - \omega_1$ and $\omega_{31} = \omega_3 - \omega_1$ are the beat frequencies of the heterodyne interference, and a mixer generates the sum frequency $\omega_{21} + \omega_{31}$. LIA1 detects the amplitude and phase of the heterodyne interference between the third-order nonlinear signal and ω_1 pulse, and LIA2 detects the amplitude of the heterodyne interference between ω_1 and ω_3 pulses. (b) Pulse sequence, with corresponding delay time τ and T. The third-order nonlinear signal is generated after the irradiation of ω_3 pulse, and the frequency is shifted by $-\omega_1 + \omega_2 + \omega_3$ that corresponds to the $-\boldsymbol{k}_1 + \boldsymbol{k}_2 + \boldsymbol{k}_3$ signal in conventional FWM measurements. Undesired signals, such as $\omega_1 - \omega_2 + \omega_3$ ($\boldsymbol{k}_1 - \boldsymbol{k}_2 + \boldsymbol{k}_3$), are removed from the frequency differences. (c) Complex FWM spectrum of a GaAs SQW at 4 K. The real and imaginary parts are denoted as Re and Im, respectively. Delay time $\tau = 0$ ps and $T = 0$ ps. ω_1, ω_2, and ω_3 were set to 40.000, 40.005, and 40.009 MHz, respectively. The reference frequency $\omega_{21} + \omega_{31}$ is 14 kHz. Solid lines are corrected using the phase shift of the reference pulse due to the reflection at the sample. Cross symbols ($\times$) are uncorrected signals. B_H and B_M indicate heavy-heavy-hole and mixed heavy-light-hole biexcitons, respectively.

$\chi^{(3)}$ and $\phi^{(3)}$ are the functions of the delay times. The first, second, and third excitation light fields before the irradiation of the sample are written as

$$\tilde{E}_n(\omega) = E_n(\omega)\exp[i(\omega+\omega_n)t + i\phi_n(\omega) + 2\pi i l_n/\lambda], \quad (6)$$

where $n = 1,2,3$. The signal of the PMT is $|\tilde{r}(\omega)\tilde{E}_1(\omega) + \tilde{r}(\omega)\tilde{E}_2(\omega) + \tilde{r}(\omega)\tilde{E}_3(\omega) + \tilde{E}^{(3)}_{\rm sig}(\omega)|^2$. In the following, we omit the argument ω. The third-order nonlinear signal $\tilde{E}^{(3)}_{\rm sig}$ is generated after the irradiation of $\tilde{E}_3$ pulse, and the frequency is shifted by $-\omega_1 + \omega_2 + \omega_3$, as shown in Fig. 2(b). The signal contains the following cross terms,

$$\begin{aligned} I_{21} &= 2r^2 E_1 E_2 \cos[\omega_{21}t + \phi_{21} + 2\pi l_{21}/\lambda], \\ I_{31} &= 2r^2 E_1 E_3 \cos[\omega_{31}t + \phi_{31} + 2\pi l_{31}/\lambda], \\ I_{s1} &= 2r\chi^{(3)} E_1^2 E_2 E_3 \cos[(\omega_{31}+\omega_{21})t + \phi^{(3)} \\ &\quad - \phi_r + \phi_{31} + \phi_{21} + 2\pi(l_{31}+l_{21})/\lambda]. \end{aligned} \quad (7)$$

Here, some cross terms with beat frequencies of ω_{21} and ω_{31} are neglected, because $\chi^{(3)} \ll r$. Parameter I_{s1} is the cross term between $\tilde{E}^{(3)}_{\rm sig}$ and $\tilde{r}\tilde{E}_1$, and the beat frequency is $(-\omega_1 + \omega_2 + \omega_3) - \omega_1 = \omega_{31} + \omega_{21}$. When the sum frequency $\omega_{31} + \omega_{21}$ between I_{31} and I_{21} generated by a mixer, as shown in Fig. 2(a), is used as the reference for LIA1, the amplitude A_1 and phase Φ_1 are written as

$$A_1 \propto r\chi^{(3)} E_1^2 E_2 E_3, \quad (8)$$

$$\Phi_1 = \phi^{(3)} - \phi_r. \quad (9)$$

When I_{31} is used as the reference for LIA2, the amplitude and phase are $A_2 \propto r^2 E_1 E_3$ and $\Phi_2 = 0$, respectively. As $E_1 \propto E_3$, $A_1/\sqrt{A_2} \propto \chi^{(3)} E_1 E_2 E_3$.

Figure 2(c) shows the typical result of the real and imaginary parts of the FWM signal. The sample is a GaAs SQW with a well thickness of 15 nm. All measurements were performed at 4 K, and the excitation pulses were collinearly polarized. The time delays were set to $\tau = 0$ ps and $T = 0$ ps. Moreover, the reflected pulse from the sample was used as the reference, as mentioned earlier. Therefore, the reference pulse includes the information of the phase shift ϕ_r, as shown in Fig. 1(c). The solid lines represent the FWM signal that is corrected using the phase shift of the reference pulse. Because ϕ_r is negligible compared to $\phi^{(3)}$, the corrected spectra (solid lines) correspond to the uncorrected spectra (cross symbols, $\times$). Note that there is a phase offset in $\phi^{(3)}$ because the absolute phase is not determined. I set $\phi^{(3)} = 0$ at the peak energy of the heavy-hole exciton. The intensity spectrum obtained from the real and imaginary parts corresponds to the previously obtained one by conventional FWM measurements [20]; the phase change with respect to the change in the delay time τ is consistent (not shown here). It is concluded that the amplitude and phase are measured correctly.

In addition to X_H and X_L, heavy-heavy-hole biexcitons (B_H) and mixed heavy-light-hole biexcitons (B_M) are observed [21]. The signs of the biexcitons, which are observed at the low-energy side of X_H and X_L, are opposite to those of the excitons because the polarization due to the transition from the biexciton to the exciton state has the opposite sign to that for the transition from an exciton to the ground state [22].

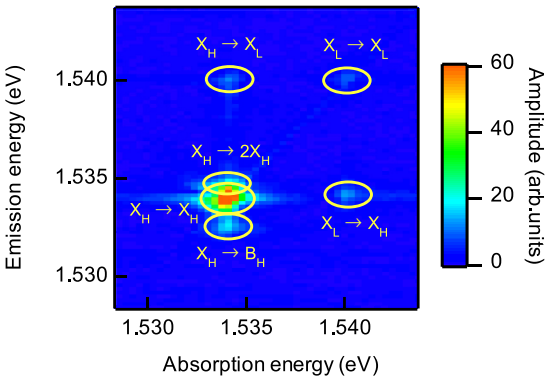

FIG. 3. 2D spectrum for rephasing pulse sequences, i.e., $\tau > 0$, in a GaAs SQW at 4 K. The excitation pulses are collinearly polarized. The delay $T = 0.2$ ps. $2X_H$ indicates the antibound two-exciton state. The arrows represent the scattering process during the pulse excitation. The delay times τ were scanned 120 points with 0.1 ps steps. The monochromator scanned 80 points with 0.1 nm steps. The measurement took 30 h. ω_1, ω_2, and ω_3 were set to 40.000, 40.005, and 40.009 MHz, respectively. The full width at half maximum of the spectral resolution is 0.14 nm, that is, 0.27 meV at the experimental condition. The spectral resolution is comparable to the step size of the monochromator.

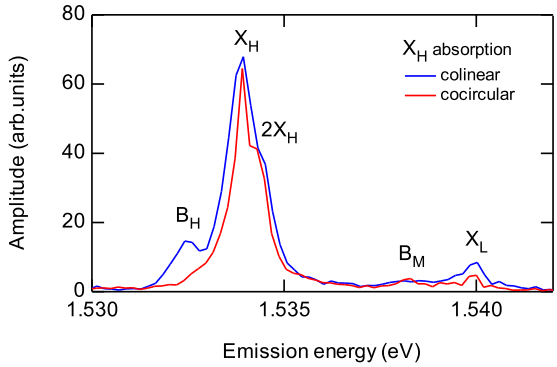

FIG. 4. Emission spectra in a GaAs SQW for collinear and cocircular configurations due to heavy-hole exciton (X_H) absorption. Excitation and reference pulses are collinearly and cocircularly polarized, respectively. B_H, B_M, and $2X_H$ correspond to a heavy-hole biexciton, mixed heavy-light-hole biexciton, and antibound two excitons, respectively.

In this method, the mechanical fluctuation of the interferometer does not affect the measurement. Essentially, the LIA multiplies the input signal and reference, passes through low-pass filters, and measures the dc component. Thus, the phase noise equivalently included in the signal and reference is removed. Therefore, we can perform the 2DCS without an active stabilization of the interferometer. In many cases, the contribution of ϕ_r is small compared with that of $\phi^{(3)}$ because the reflected light mainly comes from the substrate with no structure in the interest region. In addition, the power spectrum of the Fourier transform does not depend on ϕ_r, which is constant against the delay τ.

By performing a Fourier transform with respect to the delay τ, we obtain a 2D spectrum [23], as shown in Fig. 3. The 2D spectrum clearly presents two diagonal and two off-diagonal peaks. The diagonal peaks indicate the X_H (X_L) absorption and emission processes. The off-diagonal peaks result from the scattering of $X_H \rightarrow X_L$ and $X_L \rightarrow X_H$ during the pulse excitation process. Two peaks around the diagonal peak of X_H correspond to the B_H and antibound two-exciton ($2X_H$) states composed of two heavy-hole excitons.

To study the origin of the peaks of the 2D spectrum, their polarization dependence is measured. The emission spectra induced by X_H absorption in the collinear and cocircular configurations, as shown in Fig. 4, are obtained by integrating the 2D spectra (Fig. 3) from 1.533 to 1.535 eV with respect to the horizontal axis. The B_H peak disappears in the cocircular configuration, and the $2X_H$ and B_M peaks are observed in both configurations. The binding energies of B_H and B_M are 1.52 and 1.71 meV, respectively, which agree well with the literature values [21,24,25]. The energy difference between X_H and $2X_H$ corresponds to the interaction energy between same-spin excitons. The repulsive energy is estimated as 0.38 meV, which is larger than that in previous reports [4,26]. We attribute the lateral confinement induced by the roughness of the well thickness as a possible reason for the large repulsive energy. The localization of the excitons originating from the fluctuation of the well thickness is realized in a II-VI QW, and antibound states are observed [27]. In addition, the localization of the excitons to the quantum islands is indicated in the GaAs SQW [28]. The repulsive energy increases with decreasing lateral confinement size [29] because the repulsive energy increases with decreasing distance between the two excitons [30,31]. In our sample, it is expected that the excitons are localized to the quantum islands and the lateral confinement induces the large repulsive energy between the two excitons.

In summary, the method discussed in this Rapid Communication was demonstrated to determine the amplitude and phase of optical fields by using heterodyne interference and synchronized lock-in detection techniques. Complex reflectance spectra of a GaAs SQW are observed as typical examples of this method. The phase change of 0.01–0.05 rad is measurable without using a stable interferometer. In addition, the application of this method shows the amplitude and phase of the third-order nonlinear optical signals. By using this method, we assigned the multiexciton peaks in a GaAs SQW from the polarization dependence. The large repulsive energy of the antibound states of two excitons result from the quantum confinement induced by the roughness of the well thickness. The features of this method are as follows: (1) The measurement is not affected by the mechanical fluctuation of the interferometer. (2) The amplitude and phase of linear and nonlinear optical fields are directly obtained by using a two-phase lock-in amplifier. (3) The coaxial geometry of the excitation pulse sequences enables the use of a microscope. These features open possibilities for the many-body physics of semiconductors and single nano-objects. The modulation techniques were previously compared with the conventional 2DCS and were shown to provide different information [32]. As a remaining task, it is necessary to compare the conventional 2DCS with our method.

This work was supported by JSPS KAKENHI Grant No. JP16K05399 and partially by JP15H03765. The author thanks Y. Mitsumori and F. Minami for helpful discussions.

[1] S. T. Cundiff and S. Mukamel, Phys. Today **66**(7), 44 (2013).
[2] P. Hamm and M. Zanni, *Concept and Methods of 2D Infrared Spectroscopy* (Cambridge University Press, Cambridge, U.K., 2011).
[3] J. Shah, *Ultrafast Spectroscopy of Semiconductors and Semiconductor Nanostructures* (Springer, Berlin, 1999).
[4] R. Singh, T. Suzuki, T. M. Autry, G. Moody, M. E. Siemens, and S. T. Cundiff, Phys. Rev. B **94**, 081304(R) (2016).
[5] J. C. Vaughan, T. Hornung, K. W. Stone, and K. A. Nelson, J. Phys. Chem. A **111**, 4883 (2007).
[6] D. B. Turner, K. W. Stone, K. Gundogdu, and K. A. Nelson, Rev. Sci. Instrum. **82**, 081301 (2011).
[7] S. Shin and M. Zanni, Phys. Chem. Phys. **11**, 748 (2009).
[8] D. Birkedal, K. Leosson, and J. M. Hvam, Phys. Rev. Lett. **87**, 227401 (2001).
[9] P. Borri, W. Langbein, S. Schneider, U. Woggon, R. L. Sellin, D. Ouyang, and D. Bimberg, Phys. Rev. Lett. **87**, 157401 (2001).
[10] X. Li, T. Zhang, C. N. Borca, and S. T. Cundiff, Phys. Rev. Lett. **96**, 057406 (2006).
[11] T. Zhang, C. N. Borca, X. Li, and S. T. Cundiff, Opt. Express **13**, 7432 (2005).
[12] A. D. Bristow, D. Karaiskaj, X. Dai, T. Zhang, C. Carlsson, K. R. Hagen, R. Jimenez, and S. T. Cundiff, Rev. Sci. Instrum. **80**, 073108 (2009).
[13] P. F. Tekavec, T. R. Dyke, and A. H. Marcus, J. Chem. Phys. **125**, 194303 (2006).
[14] A. K. De, D. Monahan, J. M. Dawlaty, and G. R. Fleming, J. Chem. Phys. **140**, 194201 (2014).
[15] G. Nardin, T. M. Autry, K. L. Silverman, and S. T. Cundiff, Opt. Express **21**, 28617 (2013).
[16] K. J. Karki, J. R. Widom, J. Seibt, I. Moody, M. C. Lonergan, T. Pullerits, and A. H. Marcus, Nat. Commun. **5**, 5869 (2014).
[17] N. C. Nielsen, T. H. zu Siederdissen, J. Kuhl, M. Schaarschmidt, J. Förstner, A. Knorr, and H. Giessen, Phys. Rev. Lett. **94**, 057406 (2005).
[18] Y. Ogawa, J. Nakagawa, and F. Minami, J. Lumin. **119-120**, 399 (2006).
[19] In the two AOM setup, the frequency of the signal is a radio wave band. Because the intensity of the light after passing through the monochromator is weak, it is difficult to detect the signal of the radio frequency.
[20] Y. Ogawa, H. Tahara, and F. Minami, Phys. Rev. B **87**, 165305 (2013).
[21] L. Yang, Igor V. Schweigert, S. T. Cundiff, and S. Mukamel, Phys. Rev. B **75**, 125302 (2007).
[22] A. D. Bristow, D. Karaiskaj, X. Dai, R. P. Mirin, and S. T. Cundiff, Phys. Rev. B **79**, 161305(R) (2009).
[23] Although a long-term time delay drift with the order of the wavelength (a few femtoseconds) will exist, the drift does not affect the Fourier transform, because the delay drift is much shorter than the response time of the semiconductors (a few hundred femtoseconds).
[24] H. P. Wagner, W. Langbein, and J. M. Hvam, Phys. Rev. B **59**, 4584 (1999).
[25] B. L. Wilmer, D. Webber, J. M. Ashley, K. C. Hall, and A. D. Bristow, Phys. Rev. B **94**, 075207 (2016).
[26] M. Kuwata-Gonokami, S. Inouye, H. Suzuura, M. Shirane, R. Shimano, T. Someya, and H. Sakaki, Phys. Rev. Lett. **79**, 1341 (1997).
[27] H. Zhou, A. V. Nurmikko, C. C. Chu, J. Han, R. L. Gunshor, and T. Takagahara, Phys. Rev. B **58**, 10131(R) (1998).
[28] Y. Mitsumori, A. Hasegawa, M. Sasaki, H. Maruki, and F. Minami, Phys. Rev. B **71**, 233305 (2005).
[29] O. Heller, P. Lelong, and G. Bastard, Phys. Rev. B **56**, 4702 (1997).
[30] S. Okumura and T. Ogawa, Phys. Rev. B **65**, 035105 (2001).
[31] C. Schindler and R. Zimmermann, Phys. Rev. B **78**, 045313 (2008).
[32] G. A. Lott, A. P. Ortiz, J. K. Utterback, J. R. Widom, A. A. Guzik, and A. H. Marcus, Proc. Natl. Acad. Sci. USA **108**, 16521 (2011).